Crack-propagation sequence and pore-fluid conditions during fault-bend folding in the Appalachian Valley and Ridge, central Pennsylvania

DEEPAK C. SRIVASTAVA*
TERRY ENGELDER
Department of Geosciences, Pennsylvania State University, University Park, Pennsylvania 16802

ABSTRACT

Bedding-parallel (BPV), strike (SV), and cross-fold (CFV) veins represent a sequence of polyphase fracturing during the development of a fault-bend fold in lower Paleozoic carbonate beds in the Appalachian Valley and Ridge province, Pennsylvania. Brecciation and layer-parallel shearing played important roles in the development of the earliest vein set (BPV) which propagated prior to folding. Fluid inclusions in calcite BPV are highly saline brines (23.4 wt% NaCl) trapped at conditions close to lithostatic ($P \leq 180$ MPa, $T \leq 267$ °C). While passing through the lower kink plane of a fault-bend fold, strike joints propagated in dolomitic beds located on the extensional side of neutral surfaces. Stylolitization of strike joint surfaces accompanied slip of the hanging wall up a ramp. Renewed extension upon passing through a second kink plane led to propagation of antitaxial SV along the stylolitized joints by the crack-seal process. Slightly less saline fluids (22.4 wt% NaCl) were trapped in SV at fluid pressures ≤ 144 MPa and temperatures ≤ 217 °C. With the concurrent formation of lateral ramps, the carbonates moved to the upper flat and were subjected to strike parallel extension as manifested by the propagation of antitaxial CFV. Due to further mixing of fresh waters, the salinity of fluids forming CFV decreased (20.5 wt% NaCl) with trapping conditions at $P \leq 116$ MPa and $T \leq 179$ °C. The fluid evolution path from BPV to CFV through SV shows a modest decrease in salinity with a sharp decrease in possible trapping pressures.

INTRODUCTION

Fault-bend folds develop when a décollement surface abruptly cuts across bedding to follow a higher stratigraphic bedding plane (Suppe, 1983). On initiation of slip up the ramp, the beds in the hanging wall bend synchronously at two positions where the ramping décollement changes dip. This bending is accomplished by formation of two kink bands with one kink plane in each kink band fixed. The consequence of fixed kink planes in a fault-bend fold is that the beds must fold and subsequently unfold while moving through each fixed kink plane. Syntectonic fibers in pressure shadows have been used to document the progressive deformation as the beds move through a kink plane, up a ramp, and then through another kink plane onto a higher flat (Beutner and others, 1988). One purpose of this paper is to investigate the role of brittle fracture during the movement of beds over a thrust-fault ramp and through these kink planes. Because many of these fractures are preserved as syntectonic veins with fluid inclusions, it is also possible to gather information on pore-fluid pressure and chemistry during fault-bend folding in the central Appalachian Valley and Ridge (Fig. 1).

Folding in the Appalachian Valley and Ridge is accomplished by a combination of mechanisms, the most prominent of which are brittle fracture, stress solution, and intracrystalline flow (Groshong, 1975; Spang and Groshong, 1981; Narahara and Wiltschko, 1986). In general, previous studies of the mechanisms of folding have focused on mesoscopic folds of fourth and fifth order by Nickelsen's (1963) classification. The advantage of studying smaller order folds is that most aspects of the fold can be investigated with a modest number of thin sections. Examination of deformation mechanisms for first- and second-order folds with wavelengths on the order of several hundred meters or larger is another matter.

The fold which we examined is an east-northeasterly plunging (14°/N63°) second-order syncline (Nittany Mountain syncline, the NMS) within the Nittany anticlinorium near State College, Pennsylvania (Fig. 2). A balanced cross section through the NMS is constrained by surface geology and data from Mobil Oil No-1, Long well (Gwinn, 1970). This section resembles aspects of balanced sections to the southwest through the Birmingham Window (Faill, 1987) and to the northeast through Centre Hall (Geiser, 1988). The NMS is part of a folded horse (the Nittany Mountain horse), which is more than 10 km in length and is at least the fourth horse back from the Allegheny Front (Fig. 3). Folding of the NMS was accomplished by the emplacement of other horses under the Nittany Mountain horse. Samples for our study came from the east-northeast–striking and south-southeast–dipping northwest limb of the NMS. As seen in cross section, the samples come from a position above a flat-on-flat, with the fourth horse on the second horse back from the Allegheny Front. Local bending which affected the northwest limb of the NMS occurred during the ramping of the second horse on the first. The beds of the northwest limb have passed through a minimum of three kink planes of which the first two are to the southeast of the section shown in Figure 3.

Our study focuses on the development of fractures and veins in the Tea Creek Member of the Bellefonte Formation (Lower Ordovician) and the overlying Milroy Member of the Loysburg Formation of the Valley and Ridge province in central Pennsylvania (Chafetz, 1969; Rones, 1969). The Tea Creek Member is an aphanitic, light brownish-gray to medium gray dolomite with strata of intraclastic limestone and dolomite. The Milroy Member consists of interlayered beds (30 to 90 cm thick) of buff-gray dolomite and medium-dark gray limestone. In context of regional mechanical stratigraphy, the Tea Creek and Milroy Members belong to the relatively stiffer units comprising a duplex below the roof thrust mapped by Hermann (1984). As such this roof thrust is developed in

*On post-doctoral leave from the Department of Earth Sciences, University of Roorkee, Roorkee 247667, U.P., India.

Geological Society of America Bulletin, v. 102, p. 116–128, 15 figs., 2 tables, January 1990.

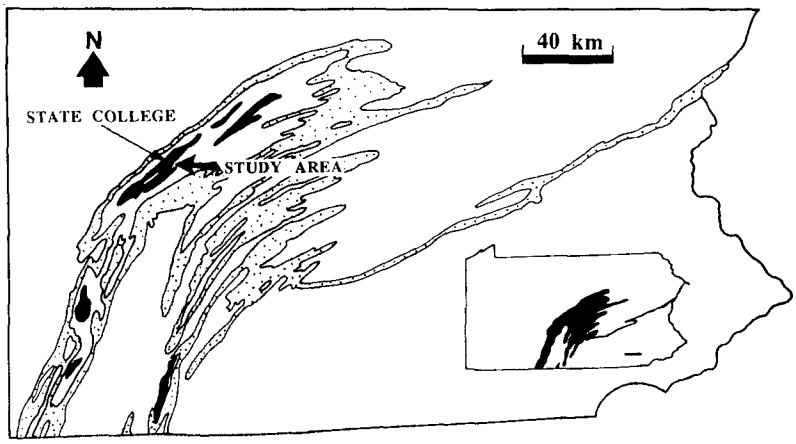

Figure 1. Location of the study area in the Valley and Ridge Province of the central Pennsylvania (black, Cambrian; dots, Silurian; blank in between black and dots, Ordovician). Inset shows the location of Valley and Ridge in Pennsylvania (black, outcrops of Valley and Ridge; length of bar is equal to 40 km).

shales belonging to the Reedsville Formation, and clastic rocks overlying it are passively folded over the carbonate duplex (Geiser, 1988).

A systematic mapping of the Tea Creek and Milroy Members reveals the presence of as many as six major sets of fractures, joints and/or veins: BPV, two types of SV, two sets of CFV and joints, and a set of neotectonic joints (Hancock and Engelder, 1989). Although the BPV dip shallowly to the southeast, the SV and CFV dip steeply and strike parallel and perpendicular to the strike of bedding, respectively (Fig. 4). Neotectonic joints are vertical and strike obliquely to bedding. The focus in this paper is on the four major sets of veins (BPV, two sets of SV, and CFV).

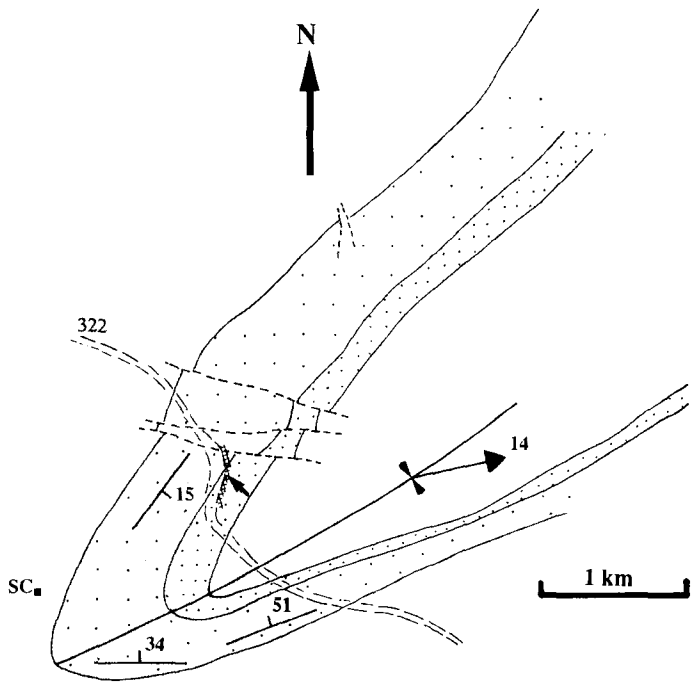

Figure 2. Geological and structural map of the Nittany Mountain syncline (sparse dots, Bellefonte Formation; dense dots, Loysburg Formation; orientation data show the dip and strike of bedding surface and the amount and bearing of plunge of Nittany Mountain syncline; dashed line, fault; dashed double line, Route 322 bypass. Cross-hachured area indicated by arrow shows outcrops for the location of samples).

MESOSCOPIC AND MICROSCOPIC CHARACTERISTICS OF THE VEINS

Bedding-Parallel Veins (BPV)

Rare BPV are characterized by brecciated geometries and undulose boundaries paralleling the bedding surfaces marked by stylolite-like dissolution seams (<1 μm thick). The microscopic geometry of these veins which fill around the clasts includes planar, pinch and swell, or one-end-tapering shapes extending parallel to the stylobedding in the host rock (Figs. 5a–5e). Veins consist of sparry calcite crystals (of 500–800 μm in longest dimension) and polygonal fragments of wall rock (Figs. 5d and 5e). Adjacent BPV are interconnected by thin offshoots (<100–300 μm) which branch off the main veins running parallel to the bedding surfaces (Fig. 5e). Their common offset along the bedding surfaces indicates layer-parallel shearing during brecciation (Fig. 5e). Between the two adjacent BPV, the offshoots typically exhibit sigmoidal or curviplanar geometries (Figs. 5b and 5c). In some places, several offshoots emerge out of the main

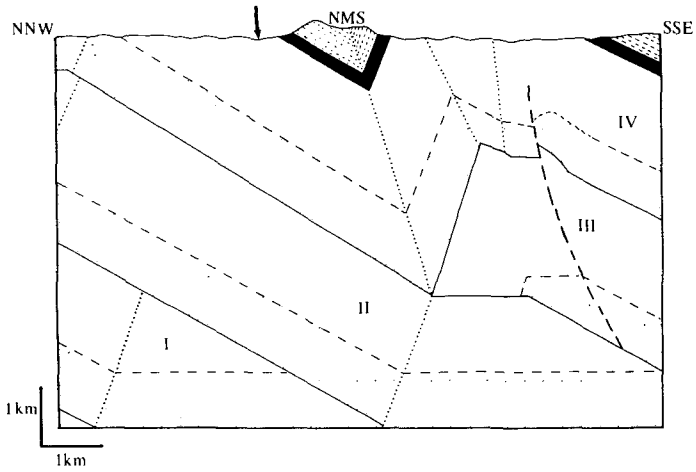

Figure 3. Cross section of structures under Nittany Mountain syncline (dots, Cambrian carbonates; blank, Ordovician carbonates; black, Reedsville shale; thin dashes, Ordovician clastics; dotted lines, traces of kink planes; thick dashed line, fault; I to IV, number of horses back from Allegheny Front; NMS, Nittany Mountain syncline. The arrows shows approximate location of outcrops on Route 322 bypass).

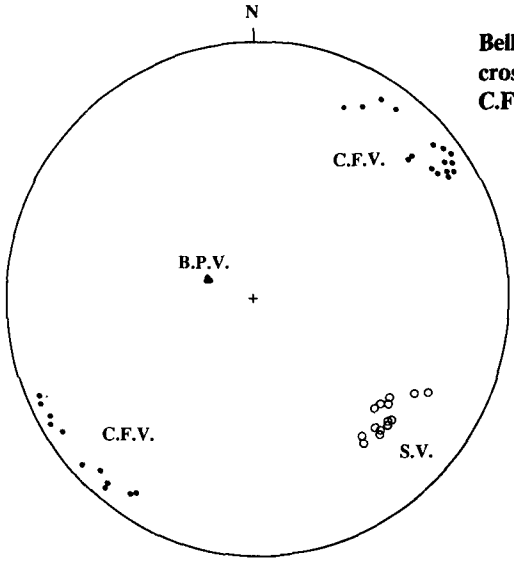

Figure 4. Lower-hemisphere projections of the poles to the fractures and veins in Bellefonte and Loysburg Formations (B.P.V., bedding-parallel veins; S.V., strike veins; C.F.V., cross-fold veins; triangles, poles to B.P.V.; open circles, poles to S.V.; filled circles, poles to C.F.V.).

vein or primary offshoots at different angles to transect the host rock, giving it a breccioid geometry (Figs. 5d and 5e; Logan and Semeniuk, 1976).

Strike Veins (SV)

These veins are most common in the dolomite beds of Milroy Member where they overprint the pre-existing BPV. Insoluble residues occur along the contacts with host rocks of some but not all SV, which on this basis are classified as stylolitic and nonstylolitic types (Fig. 6a). The presence of these insoluble residues leaves little doubt that the stylolitic SV were, at one stage in their development, the loci of stress dissolution (Alvarez and others, 1978). On outcrop scale, the average thickness, height, and spacing of stylolitic veins varies between <1–5 mm, 10–80 cm, and 30–60 cm, respectively; their vein-fill typically consists of fibrous calcite.

Four mesoscopic characteristics of stylolites suggest their development on the face of open joints. First, the stylolitic surfaces show well-preserved plumose structures (coated by insoluble residue), typical of joint propagation. Second, they are remarkably planar and cut through the beds much like a common joint. This planarity contrasts with the most common geometry for stylolites which is either undulatory or highly irregular (Alvarez and others, 1978). Third, analogous to the propagation of common joints, many stylolitic veins propagate up to but terminate at bedding boundaries (Fig. 6b; Engelder, 1985). Fourth, the stylolitic veins have a regular spacing characteristic of crack propagation in an elastic medium (Sowers, 1972). All such characteristics are consistent with stylolites developing by stress dissolution on pre-existing strike joint surfaces. Furthermore, this phenomenon has been documented on strike joints in Mississippian limestones of West Virginia (Dean and others, 1988).

SV crosscut BPV and exhibit little or no offset of the pre-existing primary structures (Figs. 6c and 6d, respectively), the latter suggesting their origin as mode I cracks. Their contact with wall rocks is characterized by the presence of insoluble residues showing nonparallel and reticulate geometries; the residues consist predominantly of carbonaceous and clay particles. In these veins, the bulk of vein-fill comprises fine fibrous calcite (2×200 μm), coarse fibrous calcite (75×200 μm), sparry calcite (125×150 to 400×600 μm), and inclusions of wall rock along with the parts of insoluble residue (Fig. 6e). In contrast to the smooth contact between adjacent fine fibers, the contact between coarse fibers is irregular, stepped, and occasionally serrated (Fig. 6f). These irregularities in the serrated contacts may represent different stages of vein growth during the development of SV by the crack-seal process (Ramsay, 1980). In most instances, the individual coarse fibers show crystallographic continuity with the groups of fine fibers crystallized on the opposite sides of coarse fiber (Fig. 6g). Evidence such as wall-to-wall crystallographic continuity of fibers, presence of zones of insoluble residues and wall-rock inclusions parallel to vein boundaries, and compositional differences between insoluble residue-seams and fibers suggest that the SV have developed by antitaxial crack seal growth (Ramsay and Huber, 1983).

Microstructural observations also indicate that the insoluble residue developed prior to any kind of filling within the veins. This stage is represented by strike fractures coated with insoluble residue but without any kind of vein material in between the surfaces of fracture and insoluble residue (Fig. 7a). Development of the insoluble residue was followed by recracking and crystallization of coarse fibers on the grains of insoluble residue. Subsequent refracturing along the contact of coarse fibers and solution seams was followed by sealing through the development of fine fibers showing opposite sense of curvatures on both sides of coarse fibers. It is noteworthy that the crystallographic orientations of groups of fine fibers are inherited from the parental coarse fibers, indicating their chrono-

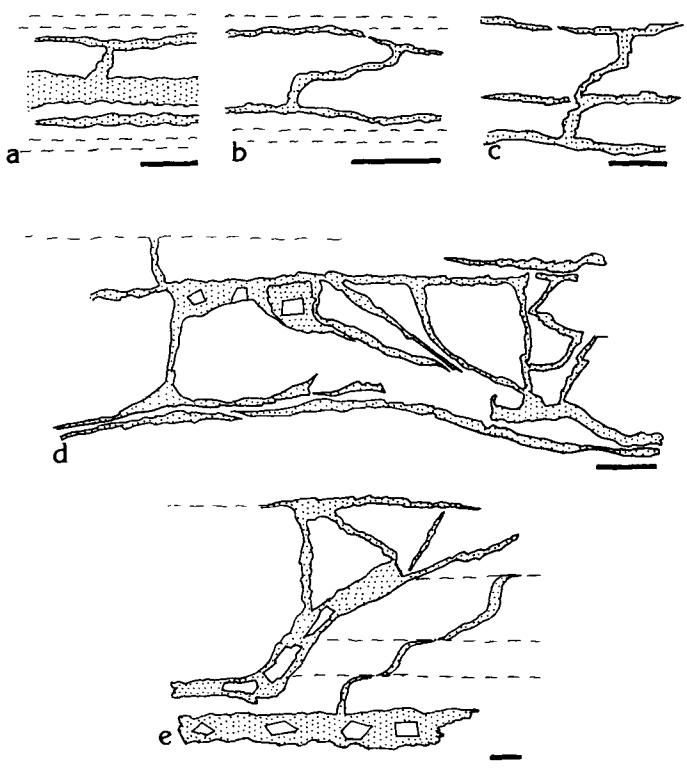

Figures 5a–5e. Hand sketches from thin sections of bedding-parallel veins (dots, veins; blank areas, host rock; blank polygons within dotted areas, wall-rock inclusions within the veins. Length of bar is equal to 1 mm in each figure).

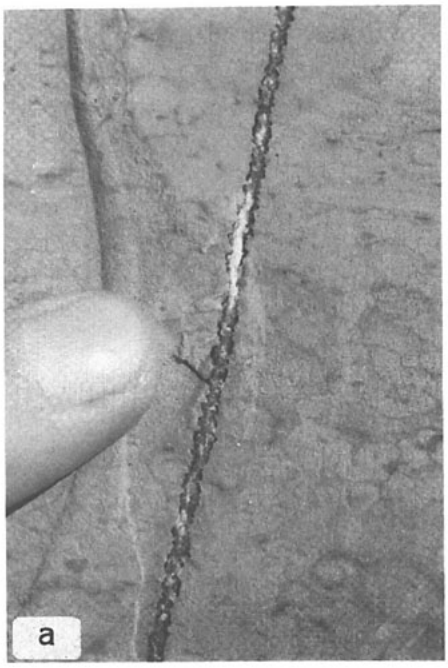

Figure 6a. Photograph of stylolitic strike vein showing the occurrence of insoluble residues at both the contacts of vein with the wall rock.

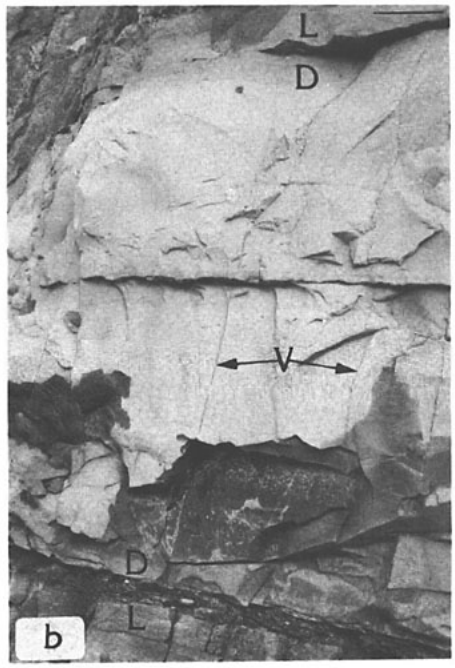

Figure 6b. Photograph of stylolitic strike vein in dolomite bed interbedded with limestone beds on top and bottom. The confinement of vein in dolomite bed and its termination at the contacts of dolomite bed with the limestone beds is noteworthy (L, limestone; D, dolomite; V, strike veins. The length of bar shown at the top right-hand corner of the photograph is equal to 10 cm).

logical development, which is antitaxial (Fig. 6g). The curvilinear geometries of the fibers imply noncoaxial deformation during the development of the SV.

Cross-Fold Veins (CFV)

The CFV propagate in both the limestone and dolomite beds and overprint the SV (Fig. 7a). In general, the average thickness of CFV varies between 1 and 2 mm and the thicker veins (a few millimeters to 2.5 cm) are restricted to small *en echelon* zones (1.5–2 m). Spacing of CFV within these zones is about 25 cm, and their height varies from 30 cm to 1 m.

Characteristically, the CFV show sharp and rectilinear boundaries and do not offset the pre-existing veins and sedimentary structures (Figs. 7b–7e). Wall-rock inclusions subparallel to the boundaries of these veins suggest successive cracking along the vein/wall contact and subsequent sealing of cracks by calcite filling (Ramsay, 1980). Although most of the CFV consist of fibrous calcite and wall-rock inclusion bands, some are filled by sparry calcite crystals. In fibrous veins, the fibers are typically rectilinear, make high angles (75°–85°) to the vein wall, and run in crystallographic continuity from wall to wall (Fig. 7b). These features suggest predominance of coaxial strain history during the development of thick CFV. In nonfibrous types of CFV, texturally diverse and deformed calcite grains are arranged systematically in different zones parallel to the vein boundaries (Figs. 7f and 7g).

Figure 6c. Photomicrograph showing overprinting relationship between strike (thick) and bedding parallel (thin) veins (plane polarized light; field of view, 2.5×2.8 mm).

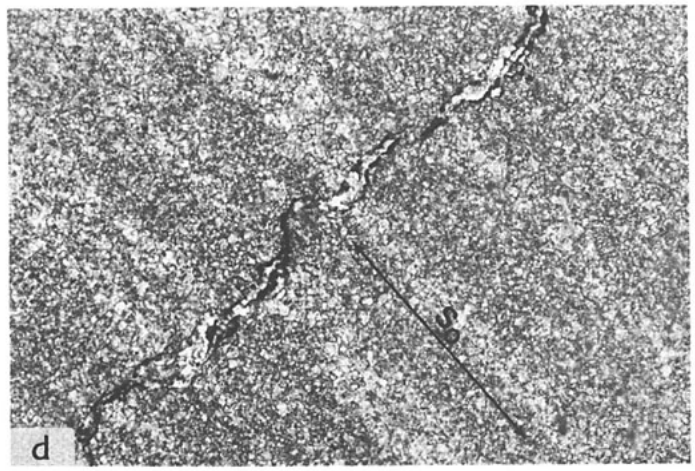

Figure 6d. Photomicrograph showing lack of offset in sedimentary layering (S_0) across a thin strike vein bordered by stress solution residues (double barbed line represents general trend of S_0; plane polarized light; field of view, 2.5×2.8 mm).

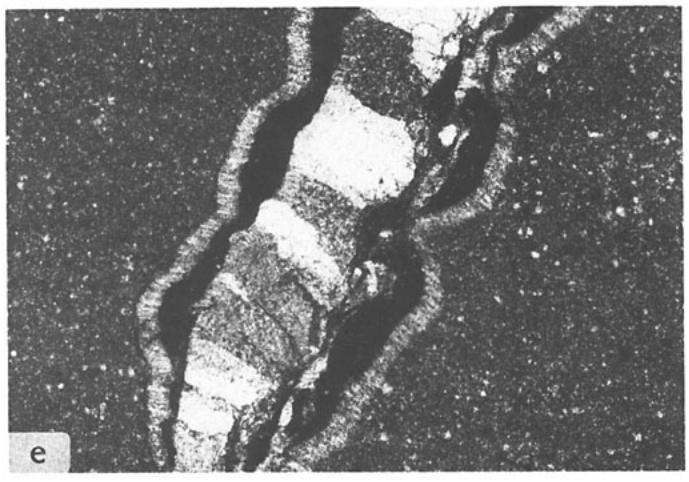

Figure 6e. Photomicrograph showing coarse fibers, zones of wall-rock inclusions with stress solution residues, and fine fibers within a strike vein (crossed nicols; field of view, 2.5×2.8 mm).

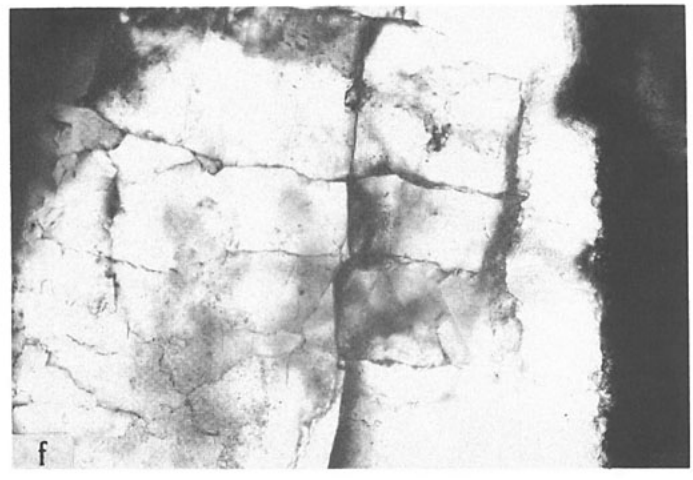

Figure 6f. Photomicrograph of strike vein showing irregular and serrated contacts between the adjacent coarse fibers (plane polarized light; field of view, 0.5×0.7 mm).

In summary, the BPV propagated first, followed by propagation of SV and CFV, respectively, in the Bellefonte and Loysburg Formations. The BPV record a component of simple shear during their development, whereas the strike and CFV propagated as extension cracks (mode I). Based on the geometry of syntectonic fibers, it can be inferred that the SV and CFV developed during broadly noncoaxial and coaxial strain histories, respectively.

FLUID INCLUSIONS

A fluid-inclusion study was undertaken to document the changes in salinity and pore-fluid pressure during the evolution of veins in the Bellefonte and Loysburg Formations. A modified U.S. Geological Survey–type heating-freezing stage manufactured by Fluid-Inc. was used for the microthermometric analysis. CFV showing the effects of deformation were not included in this study. The fluid-inclusion petrography revealed the presence of very small (generally <10 μm), two-phase (small vapor bubble in liquid phase) L-V inclusions with 85%–95% liquid by volume at room temperature in all of the veins (Figs. 8a–8d). No mono-phase, liquid, or vapor-filled inclusions were observed in any of the veins. Instances of unequivocal evidence of primary origin were rare due to absence of growth structures in calcite except in one of the sections of BPV in which distinct growth zones were observable (Fig. 8b). Daughter minerals such as halite or sylvite were typically absent in all of the inclusions.

Crushing-stage work on the many doubly polished chips containing several inclusions did not reveal the presence of compressed gasses. Crushing of some of the chips of BPV in oil, however, released several tiny bubbles (<15 μm in diameter). When parts of the same chip were crushed in kerosene, the tiny bubbles rapidly reduced in diameter and were eventually dissolved. This indicates the presence of one or more kerosene-soluble light hydrocarbons (probably methane) within the two-phase inclusions. Repeated surveys of the chips from the same sample under heating-freezing stage yielded only one monophase inclusion at room temperature, which homogenized at –86 °C and could therefore have been a methane inclusion in supercritical state at room temperature.

Fluid Salinity

On cooling of a typical two-phase inclusion, the size of the vapor bubble gradually became smaller until freezing was marked by a sudden jerk or collapse of the vapor bubble. Although the temperature was generally lowered to –150 °C (in order to detect the presence of CO_2 or CH_4), most inclusions showed complete freezing at temperatures above –60 °C. On slow warming, the appearance of "very granular" or "crazy pavy" textures marked the temperature of first melting (T_{fm}) which ranges from –30.0 to –42.0 °C (Shepherd and others, 1985). Being based on the textural criterion alone, an exact determination of T_{fm} is difficult. As the range of T_{fm} values is considerably lower than the eutectic temperature for the H_2O-NaCl system (–20.8 °C), however, the presence of other salts ($MgCl_2$) along with NaCl is inferred within the analyzed fluid inclusions (Crawford, 1981). The sodium chloride equivalent salinity (wt%) of each inclusion is determined by substituting values of melting temperature for the last ice crystal (T_m) in the equation given by Potter and others (1978). In stylolitic SV, precise determinations of T_m are difficult on account of the paucity and very small size (<3 μm) of fluid inclusions and poor optics owing to the turbidness of calcite. The average of five T_m observations, however, equals 22.6 wt% NaCl, which is close to a median of 22.4 wt% NaCl for the nonstylolitic veins. For all practical purposes, the salinity of

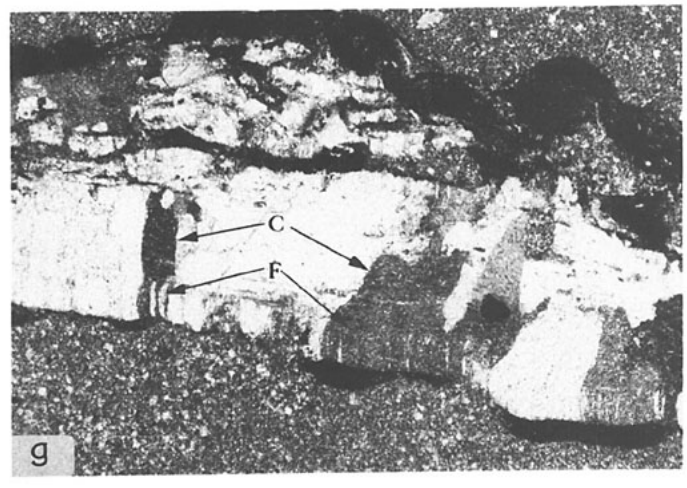

Figure 6g. Photomicrograph of strike vein showing crystallographic continuity between coarse fibers and groups of fine fibers (crossed nicols; field of view, 2.5×2.8 mm; F, fine fibers, C, coarse fibers).

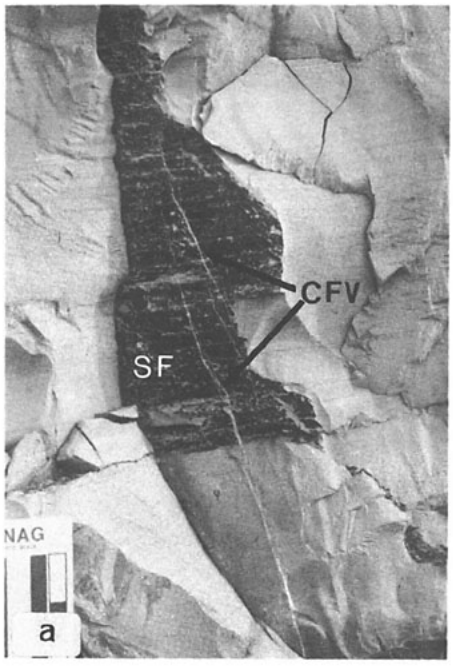

Figure 7a. Field photograph showing overprinting of cross-fold veins (CFV) on pre-existing strike fracture (SF) coated with later developed dark colored insoluble residue. No vein-fill is developed in between the surfaces of strike fracture and the insoluble residue.

Figure 7b. Photomicrograph showing sharp and rectilinear boundaries of cross-fold vein. The crystallographic continuity of fibers from wall to wall is noteworthy (crossed nicols; field of view, 2.5×2.8 mm).

Figure 7c. Photomicrograph showing crosscutting relationship between cross-fold vein (thick) and a thin strike vein (crossed nicols; field of view, 2.5×2.8 mm; arrow indicating wall-rock inclusion).

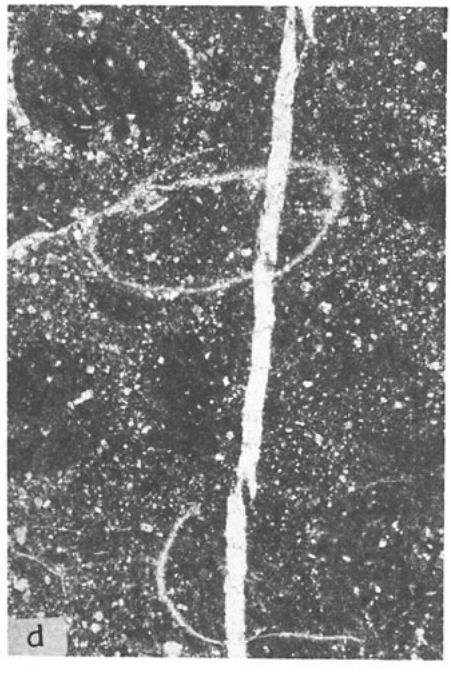

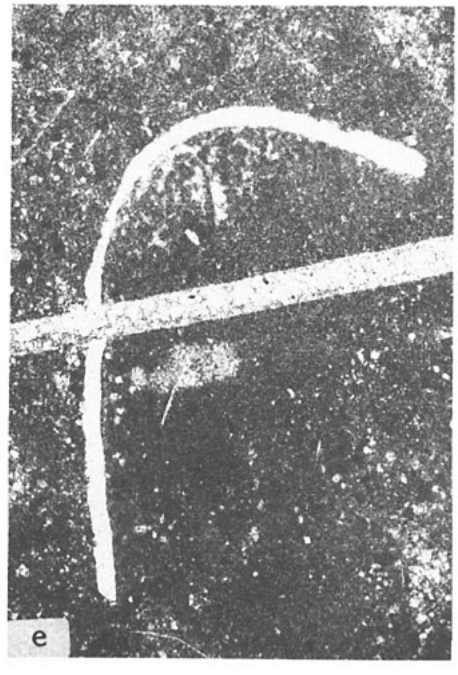

Figures 7d–7e. Photomicrographs showing lack of offset in fossils and sedimentary markers across the cross-fold veins (plane polarized light; field of view, 2.5×2.8 mm).

stylolitic veins is the same as the salinity of the nonstylolitic veins. A statistical frequency plot reveals that the salinity data for each set of veins is unimodal, and the standard deviation varies between 1.42 and 3.5 °C (Fig. 9; Table 1). The modal values of salinity for the BPV, SV, and CFV are 23.5, 22.5, and 20.5 wt% NaCl, respectively (Fig. 9). A critical comparison of these values suggests gradual decrease in salinities of brines during their evolution from older to younger veins.

Homogenization Temperatures

Heating of fluid inclusions caused a gradual reduction in size of vapor bubble and its eventual disappearance at the homogenization temperature (T_h). Repeated heating and cycling was done to obtain consistent values of T_h within a range of ±2 °C. In order to avoid the effects of stretching, necking, leaking, and resealing, T_h measurements were restricted to the

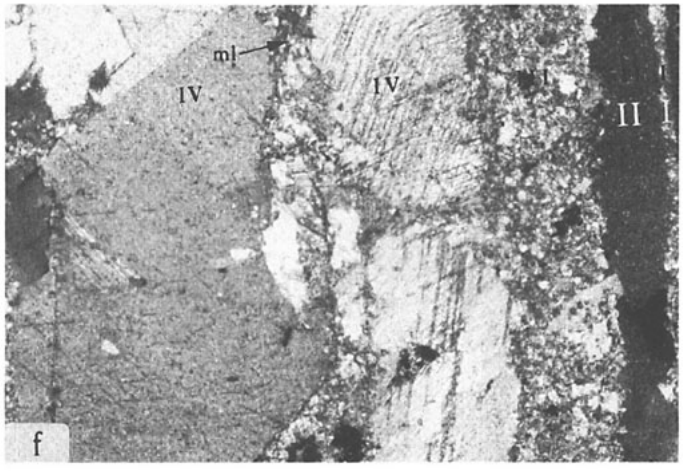

Figure 7f. Photomicrograph showing different types of calcite filling within a deformed cross-fold vein (only one-half of the mirror symmetric filling in the cross-fold vein is shown). Zones of fine-grained crushed calcite (I and III), elongated undulose and twinned calcite (II), and coarse sparry calcite (IV) are noteworthy (ml, median line; crossed nicols; field of view, 2.5×2.8 mm).

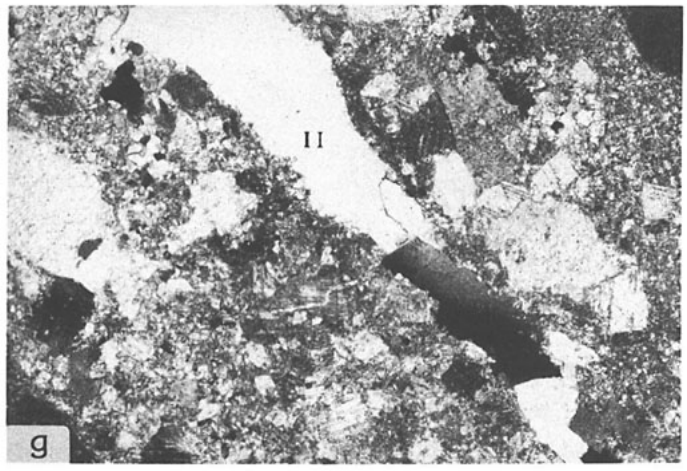

Figure 7g. Photomicrograph showing details of zone II in Figure 7f. The elongated calcite showing undulose extinction is aligned parallel to the vein boundaries trending upper-left to lower-right corner of the figure (crossed nicols; field of view, 1.1×1.5 mm).

groups of inclusions showing consistent L/V ratios (Fig. 8c). In general, the commonly occurring small inclusions (<10 μm) with consistent L/V ratios homogenized within narrow ranges of temperatures. In rarely occurring big inclusions (>30 μm), after reducing to small size (approx. <1 μm), the vapor bubble adhered to boundaries of fluid inclusions at temperatures of as much as several hundred degrees (>300 °C) and did not homogenize. Such inclusions have obviously stretched, leaked, or resealed and are excluded from the data presented during the present study. The paired T_h and T_m data (measured on same inclusion) plots in three clusters corresponding to BPV, SV, and CFV (Fig. 10). Although the clusters of SV and CFV are discrete and distinct, the cluster for BPV overlaps with that of SV. This overlapping is ascribed to the fewer number of inclusions analyzed in BPV. The clustering of data, along with the chronological order of development of veins revealed by overprinting relationships, implies that the data on T_h-T_m pairs represent three different populations corresponding to the three sets of veins in the area. A comparison of histograms showing the T_h values for fluid inclusions in different veins reveals a systematic variation in modal values (Figs. 11a–11d). The bimodal pattern in histograms for BPV and stylolitic SV may reflect the signatures of the fluids of younger veins in the older veins (Figs. 11a and 11b). The statistical summary of salinity and homogenization temperature data obtained for the different sets of veins implies gradual cooling of brines and decrease in salinities with the progressive evolution of veins (Table 1).

Trapping Conditions

The median values of T_h and T_m for three populations of data corresponding to BPV, SV, and CFV are determined and plotted graphically (Fig. 12). These data show a general decrease in salinity and homogeniza-

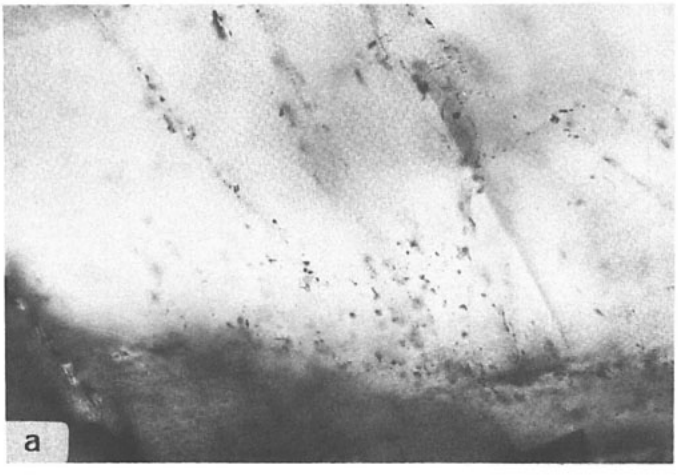

Figure 8a. Photomicrograph showing general occurrence of small two-phase (L-V) fluid inclusions in calcite veins (nonstylolitic strike vein in this case; plane polarized light; field of view, 0.3×0.5 mm).

Figure 8b. Photomicrograph showing two-phase (L-V), primary fluid inclusions along the growth zones in calcite from bedding-parallel veins (plane polarized light; field of view, 0.3×0.5 mm).

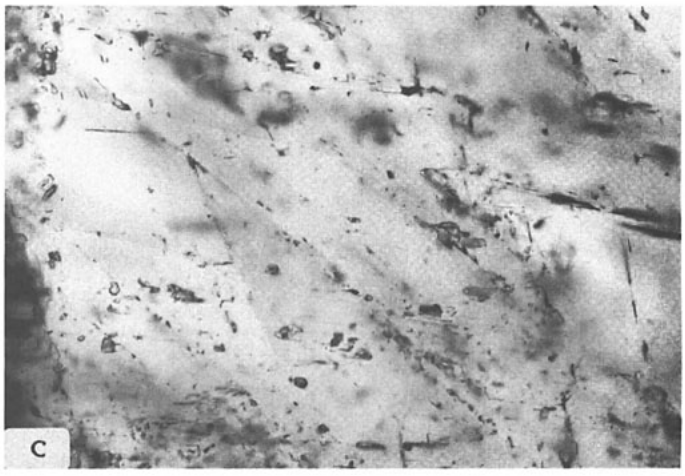

Figure 8c. Photomicrograph showing consistent liquid-vapor ratio in two-phase fluid inclusions in calcite from cross-fold vein (crossed nicols; field of view, 0.5×0.7 mm).

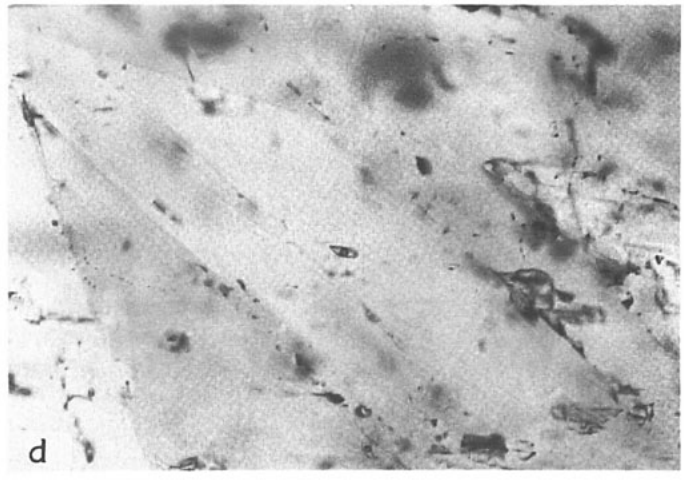

Figure 8d. Photomicrograph showing details of fluid inclusions shown in Figure 8c (plane polarized light; field of view, 0.3×0.5 mm).

TABLE 1. STATISTICAL SUMMARY OF DATA ON SALINITY AND HOMOGENIZATION TEMPERATURE

	Salinity (Wt% NaCl)				Homogenization temperature (°C)			
Vein	*No.*	*Mean*	*Median*	*S.D.*	*No.*	*Mean*	*Median*	*S.D.*
BPV	13	22.82	23.40	1.42	57	133.30	175.50	23.34
SSV	5	22.60	ND	ND	19	164.10	170.80	16.37
NSSV	40	22.20	22.40	1.95	33	147.01	148.10	11.34
CFV	92	20.76	20.55	2.07	65	128.11	125.50	23.78

Note: salinity data in wt%; homogenization temperatures in °C. Data pertain to fluid inclusions in bedding parallel (BPV), stylolitic strike (SSV), nonstylolitic strike (NSSV), and cross-fold (CFV) veins. No., the total number of analyzed fluid inclusions; S.D., standard deviation.

tion temperatures from the oldest to youngest veins (Fig. 12). Median values of data on salinity and T_h are used to calculate the density (d) of brines with the help of an equation given in Bodnar (1983).

For a given salinity, the isochores are conventionally determined by interpolation of the constants A, B, and C for a range of pressures using the

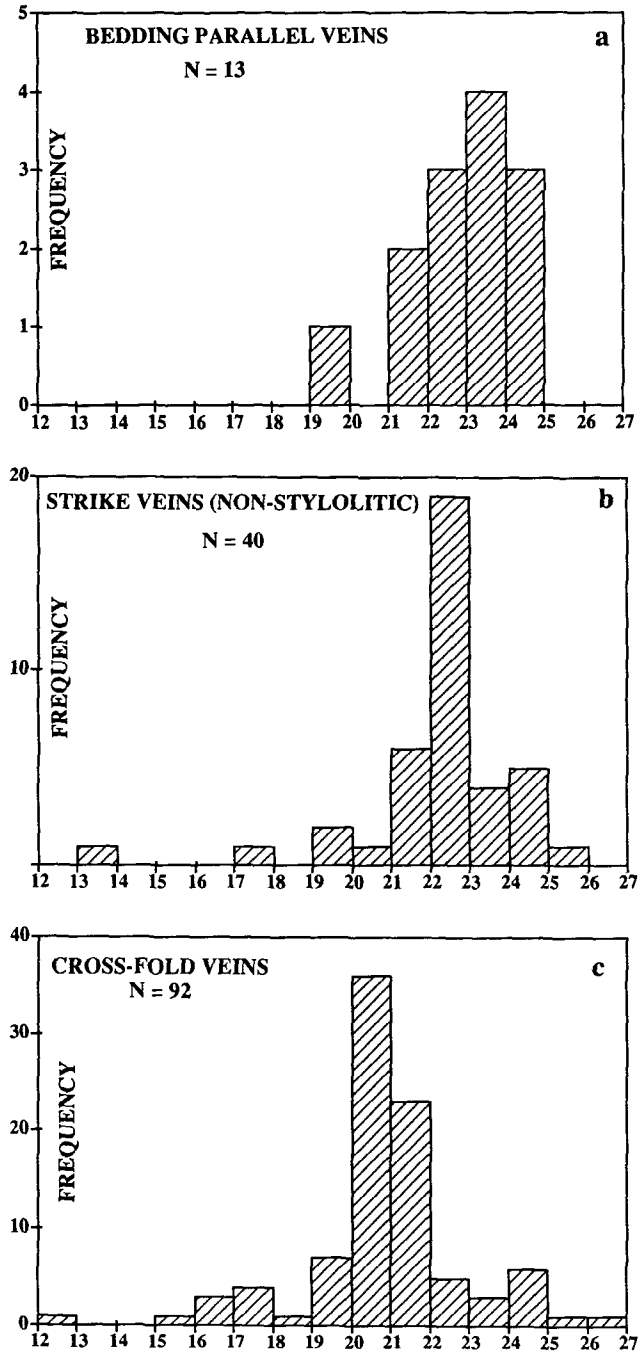

Figure 9. a, b, and c. Histograms of salinities (wt% NaCl) of fluid inclusions (L–V) in the bedding-parallel, strike (nonstylolitic), and cross-fold veins, respectively (N represents total number of observations).

regression data given in Table 29 of Potter and Brown (1977). The substitution of these constants in the equation $CT^2 + BT + (A\text{-}d) = 0$ gives different temperature values (T) corresponding to chosen values of the pressures (P) at density (d). The isochores determined by this method are nonlinear, particularly near the L-V curve, and they deviate considerably from the isochores based on experimental data on NaCl-H_2O system (Hilbert, 1979; Fig. 1 in Zhang and Frantz, 1987). Significant errors can occur in the determination of trapping conditions using isochore intersec-

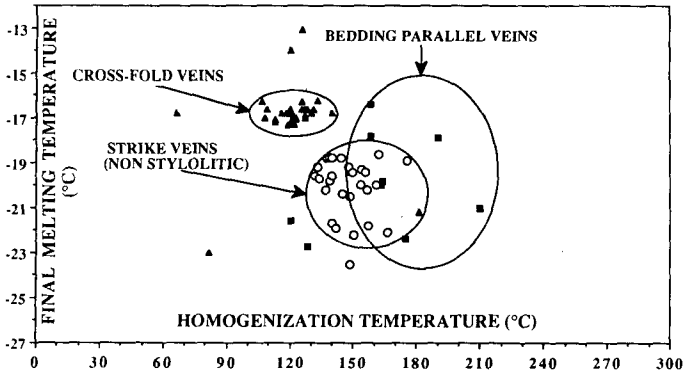

Figure 10. Graph showing the plots for final melting (Tm) and homogenization temperatures (Th) measured on the same inclusion in the bedding-parallel (rectangles), strike (circles), and cross-fold (triangles) veins.

TABLE 2. DENSITY AND TRAPPING CONDITIONS

Vein	Density (gm/cm^3)	T_t (litho) (°C)	P_t (litho) (MPa)	T_t (hydro) (°C)	P_t (hydro) (MPa)
BPV	1.059	267	180	202	52
SSV	1.058	259	174	196	50
NSSV	1.080	217	144	168	42
CFV	1.087	179	116	141	35

Note: data pertain to fluids in bedding-parallel (BPV), stylolitic strike (SSV), nonstylolitic strike (NSSV), and cross-fold (CFV) veins. T_t (litho) and P_t (litho), temperature and pressure given by intersections of the lithostatic thermobaric gradient and the respective lines of constant homogenization temperatures for the four sets of veins; T_t (hydro) and P_t (hydro), temperature and pressure given by intersections of the hydrostatic thermobaric gradient and the respective lines of constant homogenization temperatures for the four sets of veins.

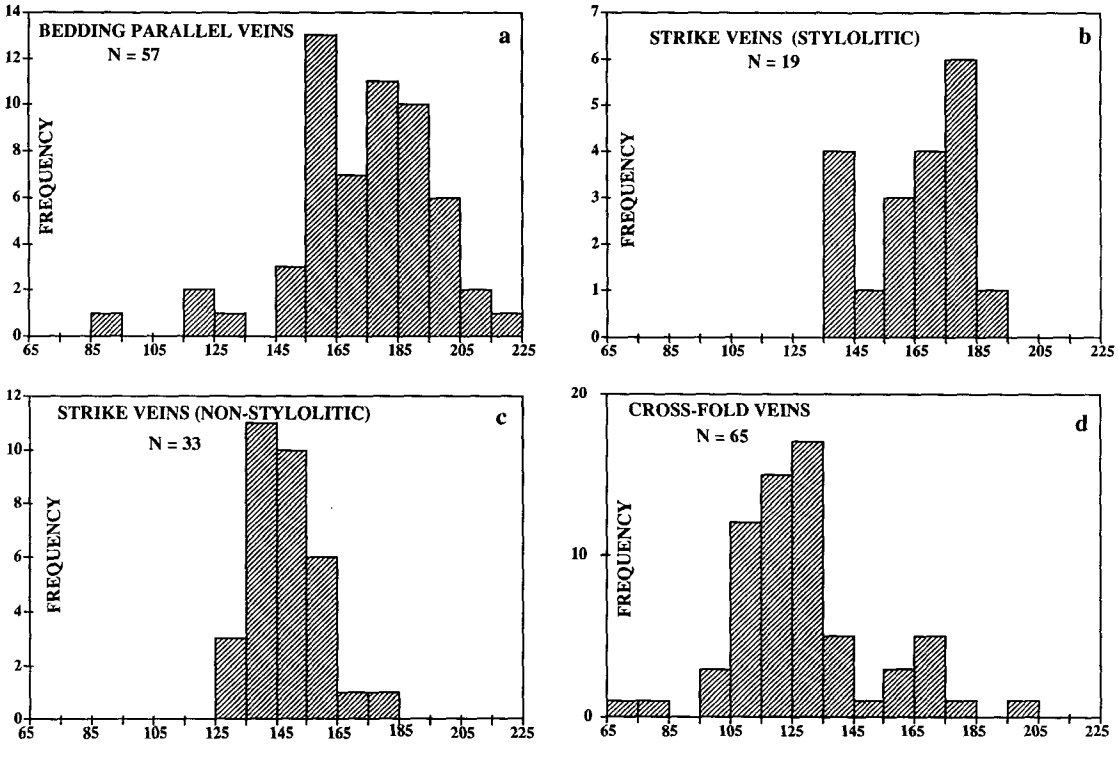

Figures 11a–11d. Histograms of homogenization temperatures (°C) of fluid inclusions (L-V) in the bedding-parallel, stylolitic-strike, nonstylolitic strike, and cross-fold veins, respectively (N represents total number of observations).

tion method and deriving the isochores from data in Potter and Brown, particularly at high densities (>1) and low pressures (<100 MPa).

Alternatively, we calculated the lines of constant homogenization temperature (LOCHT) by substituting the T_h and molality values in equation 12 given in Zhang and Frantz (1987). In P-T coordinates, this equation defines a straight line which contains the point representing trapping conditions. The highlight of Zhang and Frantz's equation is that it gives the LOCHT which match remarkably well with the experimental data on NaCl-H_2O system (Hilbert, 1979). The use of this equation does not necessitate either the assumption of constant volume or the interpolation of constants. In view of these advantages, we have calculated LOCHT using the equation $P = A_1 + A_2 T$ (Zhang and Frantz, 1987). In this equation, A_1 and A_2 are the two parameters which remain constant for a given salinity and homogenization temperature; P and T are the pressure and temperature, respectively. By substituting the values of T_h and salinity for the BPV, stylolitic SV, nonstylolitic SV, and CFV in the above mentioned equation, the respective LOCHT have been determined. These lines are represented on a P-T graph along with the arbitrary hydrostatic (3.5 °C/MPa) and lithostatic (1.37 °C/MPa) thermobaric gradients for the central Appalachians (Fig. 13).

We have inferred the pore-fluid conditions (that is, temperature, pressure, and salinity) during fault-bend folding from our fluid-inclusion study in crosscutting veins. Exact trapping conditions can be inferred only by applying an independent geothermometer or geobarometer. In the absence of additional evidence, the points of intersections of LOCHT and thermobaric gradients provide constraints on trapping conditions and, hence, the fluid pressures at the time of crack propagation during the growth of a fault-bend fold. The thermobaric gradients have been plotted for lithostatic (26 MPa/km) and hydrostatic (10 MPa/km) fluid pressures assuming a geothermal gradient of 35 °C/km (Fig. 13). Table 2 lists the

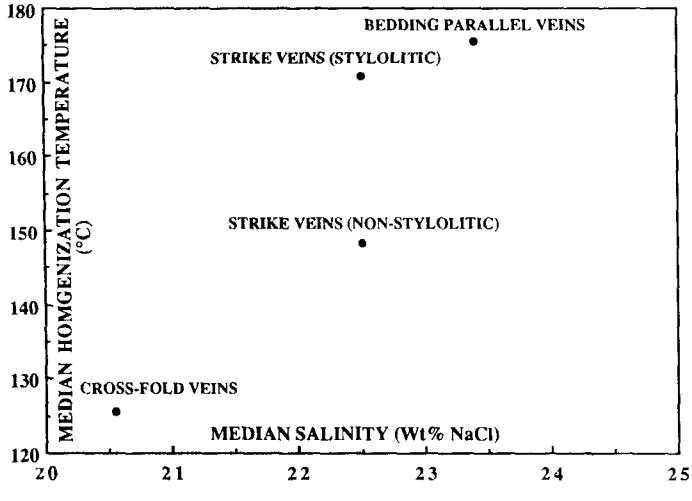

Figure 12. Graph showing plot of the median values of the salinities and homogenization temperatures for all of the analyzed fluid inclusions in the bedding-parallel, strike, and cross-fold veins.

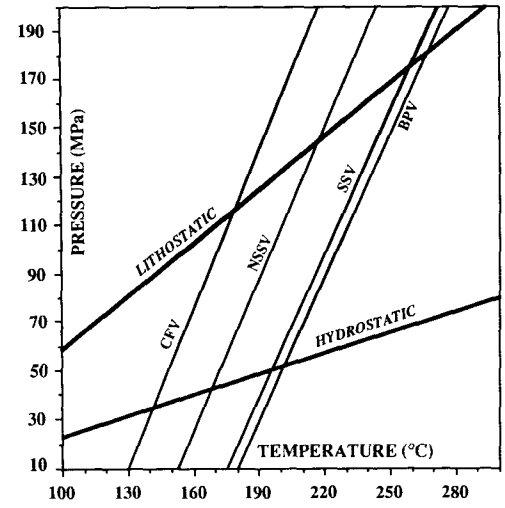

Figure 13. P-T plot showing the lines of constant homogenization temperatures for the bedding-parallel (BPV), stylolitic strike (SSV), nonstylolitic strike (NSSV), and cross-fold (CFV) veins and the lithostatic and hydrostatic thermobaric gradients.

P-T intersection points of these two thermobaric gradients and LOCHT for the four suites of fluid inclusions described above. These intersection points define hypothetical trapping pressures (P_t) and trapping temperatures (T_t).

DISCUSSION

The State of Stress Paradox during Foreland Deformation

Regional maps of contemporary tectonic stress are divided into three stress regimes based on the relative magnitude of the maximum (S_H) and minimum (S_h) horizontal stresses and vertical (S_v) stress (Zoback and Zoback, 1980). These stress regimes are named after Anderson's (1951) three fault systems with the formation of a specific system (that is, thrust, strike-slip, or normal faulting) depending on the orientation of principal stress axes (σ_1, σ_2, σ_3). The regional state of stress for thrust faulting in foreland environments such as the Appalachian Valley and Ridge should conform with the stress state was recognized by Anderson (1951) where $S_H \approx \sigma_1$, $S_h \approx \sigma_2$, and $S_v \approx \sigma_3$ (Fig. 14). Indeed, calcite-twin strain analysis of rocks on the Appalachian Plateau shows a horizontal compression and vertical extension as might be expected for $S_H \approx \sigma_1$, $S_h \approx \sigma_2$, and $S_v \approx \sigma_3$ in a thrust fault terrain (Engelder, 1979). Because veins and joints propa-

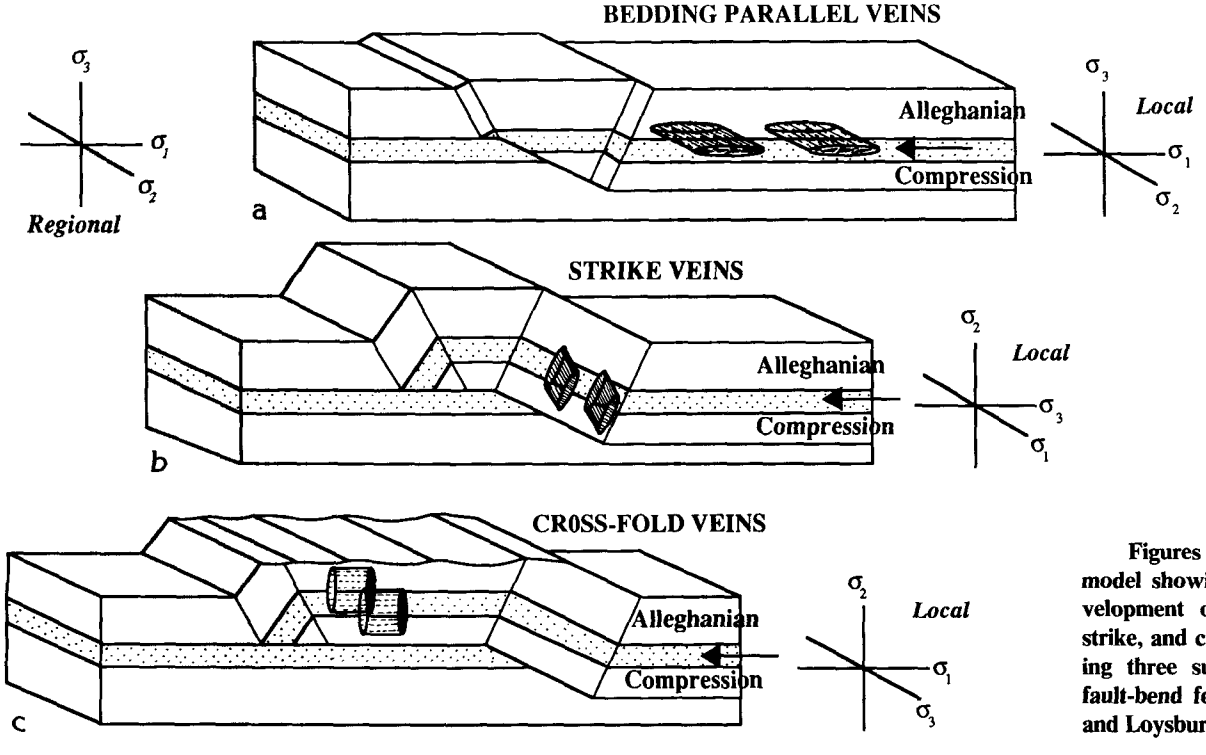

Figures 14a–14c. Schematic model showing progressive development of bedding-parallel, strike, and cross-fold veins during three successive stages of fault-bend folding in Bellefonte and Loysburg Formations.

gate normal to σ_3, the stress state for thrust faulting is compatible with the propagation of horizontal joints and veins. The examination of joint systems in foreland settings such as the Appalachian Plateau, however, leaves the initial impression that cross-fold joints and veins are the most prominent (Engelder and Geiser, 1980). Propagation of CFV is indicative of either a strike-slip ($S_H \approx \sigma_1$, $S_h \approx \sigma_3$, and $S_v \approx \sigma_2$) or normal ($S_H \approx \sigma_2$, $S_h \approx \sigma_3$, and $S_v \approx \sigma_1$) fault regime. A paradox during foreland deformation is that the stress state favoring the propagation of CFV is not compatible with that stress state favoring overthrust tectonics. Our analysis of crack-driving pressures based on fluid-inclusion trapping pressures offers a solution to this paradox.

Initial Fluid Pressure

Evidence for the fracture sequence during fault-bend folding is based on crosscutting relationships which show three distinct phases of fracturing with the development of BPV, SV, and CFV, respectively. Each vein set marks the orientation of a local stress field with σ_3 normal to the vein (Fig. 14). The earliest fracturing event was coeval with the initial development of regional thrusts in flat-lying beds. Orientation of the local stress field responsible for the development of BPV was coaxial with the regional stress field with σ_1 and σ_2 horizontal and σ_3 vertical (Fig. 14a). The earliest veins in the lower Paleozoic section of the Appalachian Valley and Ridge are commonly bedding parallel and compatible with the stress state for overthrust tectonics (Lacazette and Engelder, 1987).

Several arguments support the hypothesis that the fluid pressure during the propagation of BPV was near lithostatic ($S_v = \sigma_3$) and resulted in lifting of overburden. First, previous studies have demonstrated that the lower Paleozoic carbonates may have been buried under an overburden of more than 6 km during the Alleghanian Orogeny (Levine, 1983; Paxton, 1983; Orkan, 1986). The intersection of lithostatic thermobaric gradient and the LOCHT for the BPV indicates that fluid pressure would have lifted about 7 km of overburden during the propagation of BPV (Fig. 13). Second, fluid pressures [P_t (hydro); Table 2] indicated by the intersection of the LOCHT for the BPV and the hydrostatic thermobaric gradient line are too low for a hydrostatic water column even as short as 6 km. Third, despite their brecciated geometry, fluid would have to lift overburden during BPV development; otherwise the weight of the overburden would have caused the open pore spaces to collapse (Fig. 5). In tracking fluid pressure during the development of a fault-bend fold, evidence suggests that the initial fluid-pressure was near or at lithostatic ($P \leqslant 180$ MPa, $T \leqslant 267$ °C; Fig. 13 and Table 2).

Local Stress State due to Fault-Bend Folding

The local stress state compatible with the propagation of SV during fault-bend folding is different from the regional stress state (Fig. 14b). Although beds passed through fixed hinges of the fault-bend fold, bending forced a local stress field on the dolomite beds where σ_3 was horizontal and in the direction of the regional compression. With the development of ramps during the progression of the thrust tectonics, rocks of the Bellefonte and Loysburg Formations passed through the kink planes of fault-bend folds. Based on their present position in the fourth horse back from the Allegheny Front (see Fig. 3), these carbonates first passed through a synform at the base of a ramp. The distribution of strike veins in the Loysburg suggests that each pair of limestone-dolomite beds acted as a discrete unit during folding with a neutral surface at the contact between the limestone and dolomite (Figs. 15a and 15b). In response to extension below the neutral surface in a synform, cracks were developed in dolomite beds. Because the limestone bed was subjected to compression above the neutral surface, no cracks propagated. It is not clear why most initial cracks in the strike orientation were not filled. Vein filling occurred during extension of dolomite beds above the neutral fiber while passing through the upper fixed hinge of a fault-bend fold. This stress state caused the propagation of SV as subvertical cracks with their strikes oriented parallel to the strike of the host rocks (Fig. 14b). These SV are preserved as rare evidence for deformation of beds as they pass through the fixed hinges of fault-bend folds.

As indicated by outcrop evidence, the strike veins formed initially as cracks confined to dolomite beds (Fig. 15a). Stylolites in the Milroy Member appeared only after crack propagation accompanying folding at the first kink plane. One apparent consequence of the development of high permeability associated with these open cracks was that stress solution became active along the walls of the crack. Because no disjunctive cleavage is seen in the matrix of the dolomite, we infer that the enhanced permeability of open cracks allowed a fluid flux conducive to the development of stress solution. This association between fluid channels and the development of disjunctive cleavage has been noted in other carbonates (for example, Marshak and Engelder, 1985). Crack-seal vein formation followed the development of stylolites. Our interpretation is that these veins represent folding as the dolomite beds pass through the second kink plane at the top of the ramp. The LOCHT for the stylolitic SV is virtually the same as that for the BPV, indicating that the regional fluid circulation has not yet affected the fluids. We presume that actual trapping pressures for stylolitic SV were less than Pt (litho) for stylolitic SV (Table 2 and Fig. 13), largely because strike veins will propagate only if $S_h < S_v$. The effect of vein filling is to immediately reduce the permeability of the open crack with stylolite to the point where stress solution ceases. The LOCHT for nonstylolitic SV intersects the lithostatic thermobaric gradient at a pressure of about 140 MPa (Fig. 13). Even if these veins were trapped at maximum possible pressures (for example, 140 MPa) and before appreciable removal of overburden by erosion, they indicate a stress ratio S_h/S_v on the order of 0.78 where $S_h = \sigma_3$ and $S_v = \sigma_2$. With the removal of overburden before propagation, the stress ratio could be greater.

Evidence for Strike-Parallel Stretching

The last episode of crack propagation and vein development occurred after the carbonates were located on an upper flat. The propagation of CFV was delayed until this point as indicated by crosscutting relationships (Fig. 7a). These vertical CFV are oriented at right angles to the strike of host rocks (Fig. 14c). The local stress field responsible for development of these veins must have included a σ_3 parallel to strike so that σ_2 and σ_3 of the regional stress were interchanged at this stage. The growth of these fractures is difficult to understand in the context of an over-all thrust-fault regime and thus presents a paradox. One mechanism for the evolution of a local stress field is a horizontal contraction due to cooling and removal of overburden during syntectonic erosion. Another mechanism for reducing strike-parallel stress is strike-parallel stretching (Dan Karig, 1988, personal commun.). In the central Appalachian Valley and Ridge, rocks may stretch in the strike-parallel direction for a couple of reasons. First, as the rocks are thrust toward the craton in an arcuate fold belt, they must stretch to accommodate an increase in radius of curvature. Second, fold-thrust belts ramp in segments divided by lateral ramps. Stretching is required to

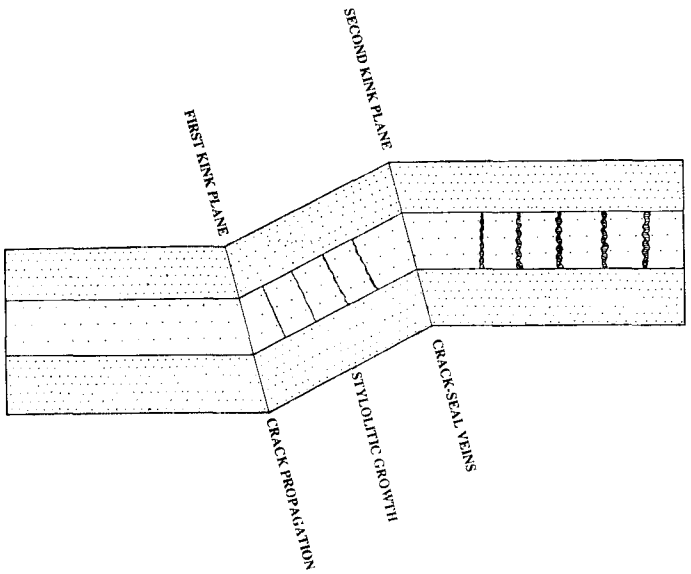

Figure 15a. Schematic diagram showing development of strike fractures, stylolites, and strike veins in the dolomite bed during fault-bend folding (sparse dots, dolomite; dense dots, limestone. The average thickness of the dolomite bed is ~1 m).

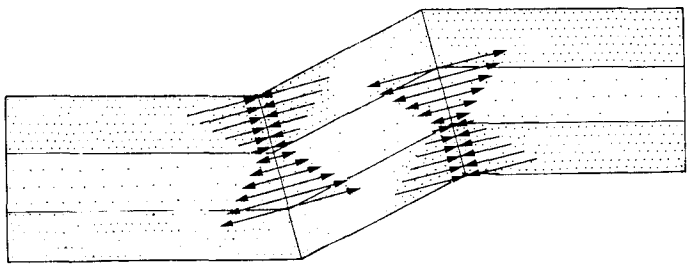

Figure 15b. Vectors show the bending forces as a pair of limestone-dolomite beds pass through the kink planes (sparse dots, dolomite; dense dots, limestone).

accommodate the lateral ramps (Alfred Lacazette, 1988, personal commun.).

The evidence that we have for strike-parallel stretching is based on the trapping pressure for CFV (Fig. 13 and Table 2). If S_h was equal to S_v during propagation of CFV, then the Pt (litho) for CFV (Table 2) indicates a maximum possible overburden of about 4.5 km. For the propagation of CFV, however, S_h has to be less than S_v, and consequently the driving pressure for CFV must have been lower than 116 MPa. From the point where fluids could lift overburden during propagation of BPV to the point where CFV propagated, the fluid pressure must have dropped more than 64 MPa [the difference in Pt (litho) of BPV and CFV; Table 2 and Fig. 13]. If erosion has kept pace with the emplacement of 2.25-km-thick carbonate sheets above roof thrusts (Fig. 3), then the overburden pressure to be removed would be on the order of 57.4 MPa [ρgh, where ρ is the average density of the upper crustal rocks (2,600 kg/m^3); g is the acceleration due to gravity (9.81 m/s^2); and h is the thickness of overburden (2.25 km)]. Thus to favor the propagation of vertical joint, S_h would have to drop more than 57.4 MPa. A drop of this magnitude cannot be achieved by the thermoelastic changes. Therefore, either the erosion was faster than the thrust-sheet emplacement, an event which we think is unlikely, or the strike-parallel stretching reduced S_h well below the overburden stress (S_v). Here again the argument is made that hydrostatic pressures do not apply because a hydrostatic column of water would be only 3.5 km tall. Our fluid-inclusion data are compatible with the hypothesis that strike-parallel stretching is the solution to the state of stress paradox within the Appalachian fold-thrust belt.

CONCLUSIONS

In the Valley and Ridge province of central Pennsylvania, the carbonate beds of Bellefonte and Loysburg Formations during fault-bend folding have recorded the imprints of three successive phases of brittle fracturing. The first phase resulted in the synchronous development of a basal flat (décollement) and brecciated BPV under similarly oriented local and regional stress fields (σ_1 and σ_2 horizontal, σ_3 vertical). Brecciated BPV were formed by highly saline brines (23.4 wt% NaCl) under conditions close to the lithostatic thermobaric gradient ($\leq$180 MPa pressure and $\leq$270 MPa temperature).

The subsequent event in the tectonic history of the region witnessed ramping of the carbonate beds and formation of fault-bend folds. During the folding at kink planes, a neutral surface developed near the contact of dolomite and limestone beds. The dolomite beds below neutral fibers were subjected to extension, causing the propagation of strike joints. While moving up the ramp, these joints were subjected to the compression resulting in development of the stylolites on the joint surfaces. While passing through a second kink plane, the stylolitized joints entered into field of extension and evolved into antitaxial veins by a crack-seal process. The development of nonstylolitic SV took place during the later extensional regime. Compositionally the fluids forming SV were less saline (22.4 wt% NaCl) and cooler than those forming BPV. The probable pressure and temperature for the development of these veins are equal to or less than 174 MPa and 259 °C, respectively.

After the carbonates had moved to the upper flat, they were subjected

to the effects of uplift and syntectonic erosion. This resulted in the propagation of antitaxial CFV which overprinted all earlier brittle structures. Due to the mixing in of fresh water, the salinity and temperature of fluid further decreased, and the approximate pressure and temperature for the formation of these veins are estimated to be 44 MPa and 173 °C, respectively.

ACKNOWLEDGMENTS

This work was supported by EPRI contract No. 2556-24 (Engelder) and National Scholarship of the Government of India (Srivastava). A. Lacazette's advice and help was critical to the success of this study. We thank A. Lacazette, R. Kerrich, and S. Wojtal for reading the earlier versions of the manuscript.

REFERENCES CITED

Alvarez, W. T., Engelder, T., and Geiser, P. A., 1978, Classification of solution cleavage in Pelagic limestones: Geology, v. 6, p. 263–266.

Beutner, E. C., Fisher, D. M., and Kirkpatrick, J. L., 1988, Kinematics of deformation at a thrust fault ramp(?) from syntectonic fibers in pressure shadows: Geological Society of America Special Paper 222, p. 77–88.

Bodnar, R. J., 1983, A method for calculation of fluid inclusion volumes based on vapor bubble diameters and P-V-T-X properties of inclusion fluids: Economic Geology, v. 78, p. 535–542.

Chafetz, H. S., 1969, Carbonates of the Lower and Middle Ordovician in central Pennsylvania: Pennsylvania Geological Survey Bulletin G58, Fourth Series, 39 p.

Crawford, M. L., 1981, Phase equilibria in aqueous fluid inclusions: Mineralogical Association of Canada, Short course hand book, 6, p. 75–100.

Dean, S. L., Kulander, B. R., and Skinner, J. M., 1988, Structural chronology of the Alleghanian orogeny in southeastern Virginia: Geological Society of America Bulletin, v. 100, p. 299–310.

Engelder, T., 1979, Mechanisms for strain within the Upper Devonian clastic sequence of the Appalachian Plateau: Western New York: American Journal of Science, v. 279, p. 527–542.

——— 1985, Loading paths to joint propagation during a tectonic cycle: An example from the Appalachian Plateau, U.S.A.: Journal of Structural Geology, v. 7, p. 459–476.

Faill, R. T., 1987, The Birmingham window; Alleghanian décollement tectonics in the Cambrian-Ordovician succession of the Appalachian Valley and Ridge province, Birmingham, Pennsylvania, *in* Roy, D., ed., Geological Society of America Centennial Field Guide, Northeastern Section, p. 37–42.

Geiser, P. A., 1988, The role of kinematics in the construction and analysis of geological cross sections in deformed terranes, *in* Mitra, G., and Wojtal, S., eds., Geometries and mechanisms of thrusting: Geological Society of America Special Paper 222, p. 47–76.

Groshong, R. H., 1975, Strain, fractures, and pressure solution in natural single-layer folds: Geological Society of America Bulletin, v. 86, p. 1363–1376.

Gwinn, V. E., 1970, Kinematic patterns and estimates of lateral shortening, Valley and Ridge Province, central Appalachians, south central Pennsylvania, *in* Fisher, G. W., Pettijohn, F. J., Reed, J. C., and Weaver, K. N., eds., Studies in Appalachian geology, central and southern: New York, Wiley-Interscience, p. 127–146.

Hancock, P. L., and Engelder, T., 1989, Neotectonic joints: Geological Society of America Bulletin, v. 101, p. 1289–1305.

Hermann, G. C., 1984, A structural synthesis of a portion of the Valley and Ridge province of Pennsylvania [M.Sc. thesis]: Storrs, Connecticut, University of Connecticut, 107 p.

Hilbert, R., 1979, PVT-daten von Wasser und von wassrigen Natriumchlorid-losungen bis 873 K, 4000 Bar und 25 Gewichtsprozent NaCl [dissert.]: Karlsruhe, West Germany, Institute of Physical Chemistry, University of Karlsruhe, 212 p.

Lacazette, A., and Engelder, T., 1987, Reducing fluids and the origin of natural fractures in the Bald Eagle Sandstone, Pennsylvania: Geological Society of America Abstracts with Programs, v. 19, p. 737.

Levine, J. R., 1983, Coal rank patterns in the Pennsylvania Anthracite region, *in* Nickelsen, R. P., and Cotter, E., eds., Silurian depositional history and Alleghanian deformation in Pennsylvania Valley and Ridge: Annual field conference of Pennsylvania geologists, 48th, Danville, Pennsylvania, Guide book, p. 67–73.

Logan, B. W., and Semeniuk, V., 1976, Dynamic metamorphism; processes and products in Devonian carbonate rocks, Canning Basin, Western Australia: Geological Society of Australia Special Publication 6, 138 p.

Marshak, S., and Engelder, T., 1985, Development of cleavage in limestones of a fold-thrust belt in eastern New York: Journal of Structural Geology, v. 7, p. 345–359.

Narahara, D. K., and Wiltschko, D. V., 1986, Deformation in the hinge region of a chevron fold, Valley and Ridge Province, central Pennsylvania: Journal of Structural Geology, v. 8 (2), p. 157–168.

Nickelsen, R. P., 1963, Fold patterns and continuous deformation mechanisms of the central Pennsylvania folded Appalachians, *in* Cate, A., ed., Tectonics and Cambro-Ordovician stratigraphy in the central Appalachians of Pennsylvania: Pittsburgh Geological Society and Appalachian Geological Society, Guide book, p. 13–29.

Orkan, N., 1986, Regional joint evaluation and paleothermometry-barometry from fluid inclusions in the Valley and Ridge province of Pennsylvania in relation to the Alleghany Orogen [M.S. thesis]: University Park, Pennsylvania, Pennsylvania State University, 130 p.

Paxton, S. T., 1983, Relationship between Pennsylvania age lithic sandstone and mudrock diagenesis and coal rank in the central Appalachians [Ph.D. thesis]: University Park, Pennsylvania, Pennsylvania State University, 503 p.

Potter, R. W., II, and Brown, D. L., 1977, The volumetric properties of aqueous sodium chloride solutions from 0 °C to 500 °C at pressures up to 2000 bars based on a regression of available data in the literature: U.S. Geological Survey Bulletin 1421-C, 35 p.

Potter, R. W., II, Clynne, M. A., and Brown, D. L., 1978, Freezing point depression of aqueous sodium chloride solutions: Economic Geology, v. 73, p. 284–285.

Ramsay, J. G., 1980, The crack-seal mechanism of rock deformation: Nature, v. 284, p. 135–139.

Ramsay, J. G., and Huber, M. I., 1983, The techniques of modern structural geology; Volume 1, Strain analysis: New York, Academic Press, 307 p.

Rones, M., 1969, A lithostratigraphic, petrographic and chemical investigation of lower Middle Ordovician carbonate rocks in central Pennsylvania: Pennsylvania Geological Survey Bulletin G53, Fourth Series, 224 p.

Shepherd, T. J., Rankin, A. H., and Alderton, D.H.M., 1985, A practical guide to fluid inclusion studies: London and Glasgow, Blackie, 239 p.

Spang, J. H., and Groshong, R. H., 1981, Deformation mechanism and strain history of a minor fold from the Appalachian Valley and Ridge Province: Tectonophysics, v. 72, p. 323–342.

Sowers, G. M., 1972, The theory of spacing of extension fractures, *in* Pincus, H., ed., Geological factors in rapid excavation: Geological Society of America Engineering Geology Case History No. 9, p. 27–53.

Suppe, J., 1983, Geometry and kinematics of fault-bend folding: American Journal of Science, v. 283, p. 684–721.

Zhang, Y., and Frantz, J. D., 1987, Determination of the homogenization temperatures and densities of supercritical fluids in the system NaCl-KCl-$CaCl_2$-H_2O using synthetic fluid inclusions: Chemical Geology, v. 64, p. 335–350.

Zoback, M. L., and Zoback, M. D., 1980, State of stress in the conterminous United States: Journal of Geophysical Research, v. 85, p. 6113–6156.

MANUSCRIPT RECEIVED BY THE SOCIETY JANUARY 12, 1989
REVISED MANUSCRIPT RECEIVED JUNE 7, 1989
MANUSCRIPT ACCEPTED JUNE 15, 1989